

OPEN ACCESS

Comparative Thermal Insulation Nature of $\text{Ca}_2\text{FeMnO}_{6-\delta}$ and $\text{Sr}_2\text{FeMnO}_{6-\delta}$

To cite this article: Ebony Schultz *et al* 2024 *ECS Adv.* **3** 014001

View the [article online](#) for updates and enhancements.

You may also like

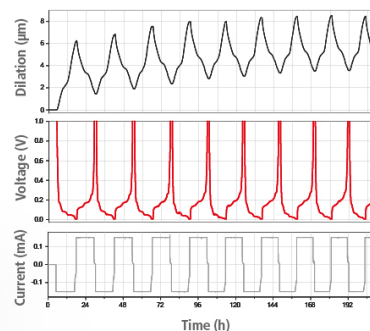
- [Evidence of cluster-glass and Griffiths-like phases in partially ordered \$\text{La}_2\text{FeMnO}_6\$ double perovskite](#)
 Mohammad Nasir, Mahmud Khan, Sunday Arome Agbo et al.
- [Bulk-sensitive Mo 4d electronic structure of \$\text{Sr}_2\text{FeMoO}_6\$ probed by high-energy Mo \$L_{2,3}\$ resonant photoemission](#)
 H. P. Martins, F. Prado, A. Caneiro et al.
- [B-site order/disorder in \$\text{A}_2\text{BBO}_6\$ and its correlation with their magnetic property](#)
 Mohd Alam and Sandip Chatterjee

Watch Your Electrodes Breathe!

Measure the Electrode Expansion in the Nanometer Range with the ECD-4-nano.

- ✓ Battery Test Cell for Dilatometric Analysis (Expansion of Electrodes)
- ✓ Capacitive Displacement Sensor (Range 250 μm , Resolution ≤ 5 nm)
- ✓ Detect Thickness Changes of the Individual Half Cell or the Full Cell
- ✓ Additional Gas Pressure (0 to 3 bar) and Temperature Sensor (-20 to 80° C)



EL-CELL[®]
 electrochemical test equipment


See Sample Test Results:



Download the Data Sheet (PDF):



Or contact us directly:

+49 40 79012-734

sales@el-cell.com

www.el-cell.com



Comparative Thermal Insulation Nature of $\text{Ca}_2\text{FeMnO}_{6-\delta}$ and $\text{Sr}_2\text{FeMnO}_{6-\delta}$

Ebony Schultz,¹ Mandy Guinn,¹ Alexa D. Azure,² and Ram Krishna Hona^{1,z} 

¹Environmental Science Department, United Tribes Technical College, Bismarck, North Dakota 58504, United States of America

²Engineering Department, United Tribes Technical College, Bismarck, North Dakota 58504, United States of America

In this study, we investigate the utility of $\text{Ca}_2\text{FeMnO}_{6-\delta}$ and $\text{Sr}_2\text{FeMnO}_{6-\delta}$ as materials with low thermal conductivity, finding potential applications in thermoelectrics, electronics, solar devices, and gas turbines for land and aerospace use. These compounds, characterized as oxygen-deficient perovskites, feature distinct vacancy arrangements. $\text{Ca}_2\text{FeMnO}_{6-\delta}$ adopts a brownmillerite-type orthorhombic structure with ordered vacancy arrangement, while $\text{Sr}_2\text{FeMnO}_{6-\delta}$ adopts a perovskite cubic structure with disordered vacancy distribution. Notably, both compounds exhibit remarkably low thermal conductivity, measuring below $0.50 \text{ W m}^{-1} \text{ K}^{-1}$. This places them among the materials with the lowest thermal conductivity reported for perovskites. The observed low thermal conductivity is attributed to oxygen vacancies and phonon scattering. Interestingly as SEM images show the smaller grain size, our findings suggest that creating vacancies and lowering the grain size or increasing the grain boundaries play a crucial role in achieving such low thermal conductivity values. This characteristic enhances the potential of these materials for applications where efficient heat dissipation, safety, and equipment longevity are paramount.

© 2024 The Author(s). Published on behalf of The Electrochemical Society by IOP Publishing Limited. This is an open access article distributed under the terms of the Creative Commons Attribution 4.0 License (CC BY, <http://creativecommons.org/licenses/by/4.0/>), which permits unrestricted reuse of the work in any medium, provided the original work is properly cited. [DOI: [10.1149/2754-2734/ad27dc](https://doi.org/10.1149/2754-2734/ad27dc)]



Manuscript submitted January 15, 2024; revised manuscript received January 27, 2024. Published February 19, 2024.

Ongoing research endeavors aim to enhance the thermal insulation properties of materials crucial for heat-based equipment like aerospace turbines and airplane blades, thereby ensuring safety and longevity. Various materials, including titanate-based ceramics,¹ composite materials,² zirconia, yttria-based materials,³ and others, have been extensively studied to achieve low thermal conductivity. Materials with low thermal conductivity are widely used in thermoelectrics as well.^{4,5} This quest for low thermal conductivity extends to diverse material classes such as perovskite oxides, pyrochlore,¹ nanophase,⁶ and Zintl phases of intermetallics.⁷ Numerous methods, including coating, alloy formation, and introducing twin interfaces, have been employed to reduce thermal conductivity. Ceramic-based oxides, particularly perovskite oxides, have garnered significant attention due to their high melting points.⁴

Perovskite oxides, denoted by the general formula ABO_3 , where A and B represent alkaline Earth or rare Earth metal and transition metal, respectively, possess an ideal cubic structure. Strategies for reducing the thermal conductivity of perovskite oxides involve inducing oxygen vacancies in the crystal lattice, lattice distortions, grain size reduction, and introducing grain boundaries. Oxygen-deficient perovskites are expressed as ABO_{3-x} or $\text{A}_2\text{B}_2\text{O}_{6-\delta}$, where x and δ represent oxygen vacancy concentration. The arrangement of vacancies in these materials can be ordered or disordered, influencing their structural flexibility and resulting in different crystal structures.⁸⁻¹¹

Phonons are quantized vibrational modes of the crystal lattice, and they are the primary carriers of heat in insulating materials. In perovskite oxides, the lattice structure and phonon interactions strongly influence thermal conductivity. Defects, grain boundaries, and other structural features can scatter phonons, affecting their ability to transport heat. Phonon scattering, which can be increased through methods like vacancy generation, boundary increment, impurity introduction, and lattice distortion, plays a crucial role in reducing thermal conductivity.^{12,13} Notably, the generation of oxygen vacancies has proven effective in lowering thermal conductivity, and its impact is often more pronounced than other contributions.^{4,13-15} Some common strategies applied to suppress the lattice thermal conductivity of thermoelectric materials include not only introducing defects^{16,17} but also alloying,¹⁸ creating nanostructures,¹⁹ and forming substructures.²⁰ One example is the

ultralow thermal conductivity captured in Na_2TlSb due to the soft Tl-Sb bonding and resonant bonding in the pseudo cage composed of the Na and Sb atoms interaction.²¹ The report explains the strong quartic anharmonicity and temperature dependence of the Tl atom with rattling behavior playing an important role in the lattice stability of Na_2TlSb . The report mentioned the finding that soft Tl-Sb bonding and resonant bonding in the pseudo cage composed of the Na and Sb atoms interaction was responsible for ultralow thermal conductivity.²¹ Strong anharmonic phonon scattering was reported in Li_2NaBi also as a cause for the lattice thermal conductivity.²²

This study focuses on oxygen-deficient perovskites, specifically $\text{Ca}_2\text{FeMnO}_{6-\delta}$ and $\text{Sr}_2\text{FeMnO}_{6-\delta}$, to explore their thermal insulation properties. The compounds were synthesized using solid-state reaction at high temperatures, and their crystal structures were determined through Rietveld refinement of powder X-ray diffraction. Both materials exhibit different arrangements of oxygen vacancies, leading to distinct coordination geometries and crystal structures. $\text{Ca}_2\text{FeMnO}_{6-\delta}$ features tetrahedral layers alternating with octahedral layers, forming a brownmillerite-type structure,²³ while $\text{Sr}_2\text{FeMnO}_{6-\delta}$ showcases random vacancy distribution resembling cubic perovskite structure.²³

Experimental

The synthesis of $\text{Ca}_2\text{FeMnO}_{6-\delta}$ and $\text{Sr}_2\text{FeMnO}_{6-\delta}$ involved the utilization of SrCO_3 , CaCO_3 , Mn_2O_3 , and Fe_2O_3 powders. These powders were meticulously weighed and thoroughly mixed in stoichiometric proportions using an agate mortar and pestle. Subsequently, the resulting mixture was compressed into pellets under a pressure of 3 tons. The pellets underwent calcination at $1000 \text{ }^\circ\text{C}$ for 24 h [MTI furnace], followed by cooling to room temperature. After cooling, the pellets were reground and repelletized. Sintering of the pellets was carried out at $1200 \text{ }^\circ\text{C}$ for 24 h, and the heating and cooling rate for both calcination and sintering processes was maintained at $100 \text{ }^\circ\text{C/h}$.

To assess the crystal structure and phase purity of the samples, Bruker X-ray diffractometer D2 Phaser was employed for powder X-ray diffraction (PXRD), using $\text{Cu K}\alpha 1$ and $\text{K}\alpha 2$ radiations with a wavelength (λ) of 1.54056 \AA . Rietveld refinements of the XRD data were conducted using GSAS software (Larson and Von Dreele 1994) along with the EXPEGUI interface (Toby 2001). Microstructure analysis was performed through scanning micrographs.

^zE-mail: rhona@uttc.edu

The concentration of oxygen vacancies in the materials was determined through iodometric titrations. In this process, 2 g of potassium iodide was mixed with 50 mg of the sample in 100 ml of 1 M HCl. A portion of the resulting solution was titrated against 0.025 M $\text{Na}_2\text{S}_2\text{O}_3$, with the addition of 0.2 ml of a starch solution as an indicator. The entire experiment was conducted under an argon atmosphere.

The thermal conductivities of the materials were studied using a Thermtest thermal conductivity meter, MP-2 with TPS-4, based on the Transient Plane Source Method. Circular discs with diameters of 13 mm and/or 25 mm and a thickness of 3 mm were placed on the flat sensor, and the thermal conductivity was measured at room temperature.

Results and Discussion

Structural analysis.—The crystal structures of the two materials, $\text{Ca}_2\text{FeMnO}_{6-\delta}$ and $\text{Sr}_2\text{FeMnO}_{6-\delta}$ have been previously documented. As reported, $\text{Ca}_2\text{FeMnO}_{6-\delta}$ exhibits a brownmillerite type compound characterized by tetrahedral layers alternating with octahedral layers, as depicted in Fig. 1. Within each tetrahedral layer, the orientation is opposite to that of the nearest layer, both above and below. This results in the alternating arrangement of tetrahedral layers, as illustrated in the inset of Fig. 1. The space group for $\text{Ca}_2\text{FeMnO}_{6-\delta}$ is $Pnma$, as detailed in Fig. 1 and Table I, which present the Rietveld refinement profile and parameters, respectively.

A structural variation arises when Sr^{2+} replaces Ca^{2+} , leading to differences in the ionic radii. This substitution induces distinct oxygen vacancy arrangements, thereby altering the coordination geometry around the B cation. In $\text{Sr}_2\text{FeMnO}_{6-\delta}$, octahedra form around Fe/Mn, as depicted in the inset of Fig. 2, deviating from the tetrahedral coordination geometry observed in $\text{Sr}_2\text{FeMnO}_{6-\delta}$. The cubic crystal structure of $\text{Sr}_2\text{FeMnO}_{6-\delta}$ is characterized by the $Pm\bar{3}m$ space group, as shown in Fig. 2 and detailed in Table II.

Figure 3 presents scanning electron microscope (SEM) micrographs of $\text{Ca}_2\text{FeMnO}_{6-\delta}$ and $\text{Sr}_2\text{FeMnO}_{6-\delta}$, illustrating their microstructures. These images highlight distinct grain geometries and growth styles in the materials, consistent with the anticipated structural variations. The grain size is significantly smaller for $\text{Sr}_2\text{FeMnO}_{6-\delta}$ than $\text{Ca}_2\text{FeMnO}_{6-\delta}$ which increases the boundaries in $\text{Sr}_2\text{FeMnO}_{6-\delta}$.

Thermal Conductivity

The thermal conductivities of both materials were investigated, revealing values below $0.50 \text{ Wm}^{-1}\text{K}^{-1}$ at room temperature. $\text{Sr}_2\text{FeMnO}_{6-\delta}$ demonstrated a lower thermal conductivity with the value of $0.36 \text{ Wm}^{-1}\text{K}^{-1}$, representing one of the lowest reported values for perovskite oxide materials. Figure 4 and Table III show the comparative thermal conductivities of the materials. This finding underscores the relationship between the grain size and reduced thermal conductivity. The synthesis method and environment were consistent with those used for previously reported perovskite oxides.²³ This study contributes to the understanding of the role of

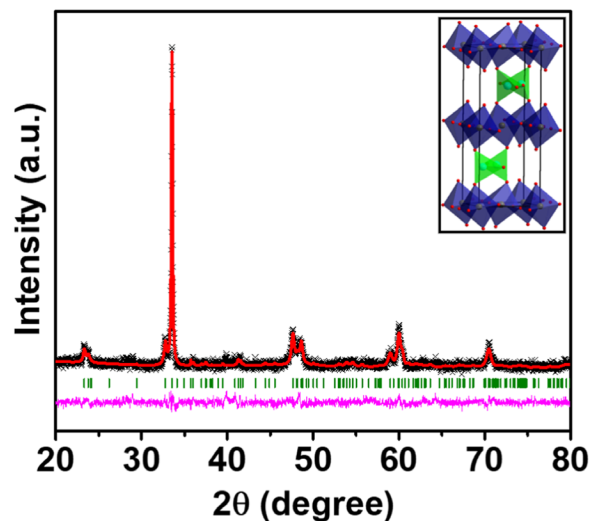


Figure 1. The Rietveld refinement profile of $\text{Ca}_2\text{FeMnO}_{6-\delta}$. The black cross, red line, green vertical lines, and pink solid line represent the raw data, the model, Bragg peak positions, and difference plot, respectively. The inset shows the crystal structure with an orthorhombic unit cell and $Pnma$ space group.

vacancy and boundary in the context of thermal insulation properties, a dimension that has received limited attention thus far.

The evaluation of thermal conductivity (K) was conducted using the Thermtest thermal conductivity meter, MP-2 with TPS-4, based on the Transient Plane Source Method. This method employs a plane sensor, a mathematical model describing heat conductivity, and electronic components to measure Thermal Transport Properties effectively. To ensure the reliability of the equipment, the thermal conductivity of a standard Pyrex verification sample was measured, yielding a value of $1.117 \text{ Wm}^{-1}\text{K}^{-1}$, consistent with the instruction manual and validating the thermal conductivity data for the studied materials.

Previous attempts to reduce thermal conductivity in perovskite oxides involved A-site or B-site cation substitution.^{4,14,15} In our study, A-cations were substituted, leading to a structural transformation. The lower thermal conductivity of our materials can be attributed to various factors, including oxygen vacancy, lattice distortion, grain size, and boundary effects. Structural transformation due to A-cation substitution rules out lattice distortions as a significant contributor to phonon scattering. Scanning electron microscopy (SEM) images indicated well-sintered materials with micrometer-sized grains, which are essential for low lattice thermal conductivity due to increased phonon scattering. Since grain boundaries can contribute to phonon scattering, the observed clear grain boundaries in both materials were focused for a significant difference of thermal conductivity. As seen in the SEM images, the grains are smaller for $\text{Sr}_2\text{FeMnO}_{6-\delta}$ which has relatively lower value of thermal conductivity.

Table I. Rietveld refinement parameters of $\text{Ca}_2\text{FeMnO}_{6-\delta}$.

Element	x	y	z	Uiso	Multiplicity	Occupancy
Ca	0.495981	0.133570	-0.051958	0.042380	8	1
Fe1	0.0000	0.0000	0.0000	0.014069	4	0.5
Mn1	0.0000	0.0000	0.0000	0.014069	4	0.5
Fe2	0.465613	0.2500	0.533668	0.046658	4	0.5
Mn2	0.465613	0.2500	0.533668	0.046658	4	0.5
O1	0.289757	-0.002798	0.174856	0.026796	8	1
O2	0.049616	0.165703	0.081423	0.097407	8	1
O3	0.687468	0.2500	-0.307780	0.002865	4	1

Space group = $Pnma$, $a = 5.334244 \text{ \AA}$, $b = 14.969558 \text{ \AA}$, $c = 5.461733 \text{ \AA}$, $wRp = 0.0376$, $Rp = 0.0296$

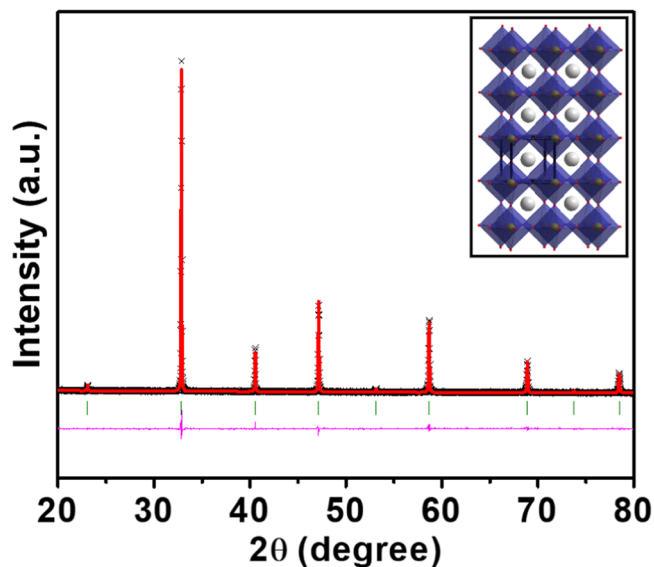


Figure 2. The Rietveld refinement profile of $\text{Sr}_2\text{FeMnO}_{6-\delta}$. The black cross, red line, green vertical lines, and pink solid line represent the raw data, the model, Bragg peak positions, and the difference plot, respectively. The inset shows the crystal structure with a cubic unit cell and $Pm\bar{3}m$ space group.

The materials, $\text{Ca}_2\text{FeMnO}_{6-\delta}$ and $\text{Sr}_2\text{FeMnO}_{6-\delta}$, have been extensively studied for their structures and charge transport properties, demonstrating different charge transport behaviors at room temperature.²³ However, the thermal conductivity difference between the two materials suggests an insignificant contribution of charge carriers to thermal conductivity. Fe^{3+} and Fe^{4+} or Mn^{3+} and Mn^{4+} spins may play a role, but their contribution appears insignificant compared to the dominant effect of phonon scattering.

The total thermal conductivity (K) is the sum of contributions from phonons (K_p) and radiation (K_R).^{24,25} As discussed earlier, phonon scattering contributes to a decrease in thermal conductivity. Local lattice distortions, void spaces, and random vacancies act as sites for phonon scattering, leading to reduced thermal conductivity. The low thermal conductivity of our materials can be attributed to the suppression of lattice thermal conductivity and increased phonon scattering due to oxygen vacancies. The oxygen vacancy (δ) values for $\text{Ca}_2\text{FeMnO}_{6-\delta}$ and $\text{Sr}_2\text{FeMnO}_{6-\delta}$ are 1.0 and 0.22, respectively,

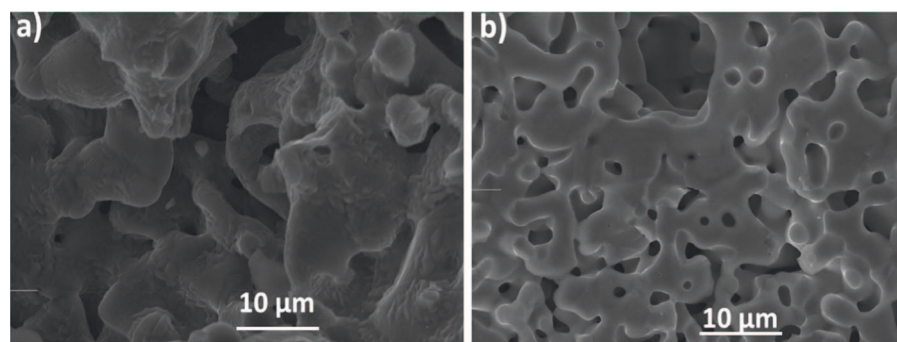


Figure 3. SEM images of (a) $\text{Ca}_2\text{FeMnO}_{6-\delta}$ (b) $\text{Sr}_2\text{FeMnO}_{6-\delta}$.

Table II. Rietveld refinement parameters of $\text{Sr}_2\text{FeMnO}_{6-\delta}$.

Element	x	y	z	Uiso	Multiplicity	Occupancy
Sr1	0.5000	0.5000	0.5000	0.023990	1	1.000
Mn1	0.0000	0.0000	0.0000	0.026154	1	0.500
Fe1	0.0000	0.0000	0.0000	0.026154	1	0.500
O1	0.5000	0.5000	0.5000	0.033145	3	0.963

Space group = $Pm\bar{3}m$, $a = 3.85051(5)$ Å, $wRp = 0.0387$, $Rp = 0.0300$

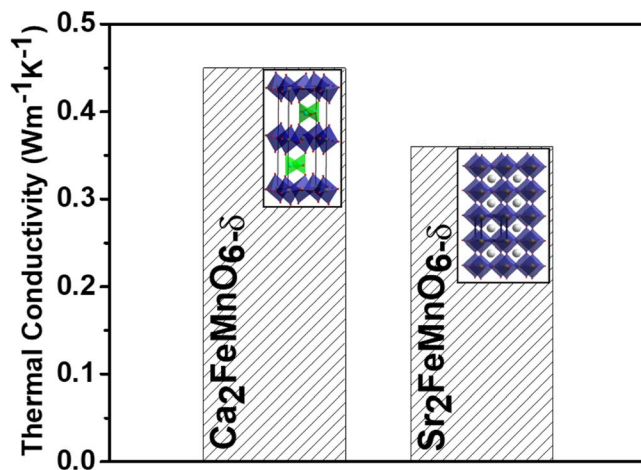


Figure 4. Comparative thermal conductivity of $\text{Ca}_2\text{FeMnO}_{6-\delta}$ and $\text{Sr}_2\text{FeMnO}_{6-\delta}$.

emphasizing the role of oxygen vacancies in lowering thermal conductivity.^{23,25}

In conclusion, the low thermal conductivity of our compounds is primarily attributed to the significant impact of oxygen vacancies on increasing phonon scattering, emphasizing their crucial role in modulating thermal conductivity. The observed difference in thermal conductivity between $\text{Ca}_2\text{FeMnO}_{6-\delta}$ and $\text{Sr}_2\text{FeMnO}_{6-\delta}$ suggests that random vacancy distribution and smaller grain size or increased grain boundaries may further contribute to this difference in thermal conductivity, leading to the lower value of $\text{Sr}_2\text{FeMnO}_{6-\delta}$.

Conclusions

In conclusion, the study on $\text{Ca}_2\text{FeMnO}_{6-\delta}$ and $\text{Sr}_2\text{FeMnO}_{6-\delta}$ highlights their low thermal conductivity, a crucial attribute for effective thermal insulation. A-cation substitution induces structural transformations, ruling out lattice distortions as a significant contributor to phonon scattering. Well-sintered materials with micrometer-sized grains, observed through SEM, contribute to increased phonon scattering and lower thermal conductivity. Charge carriers, Fe^{3+} and Fe^{4+} spins, play a limited role, with the dominant effect of phonon scattering evident in the observed thermal conductivity difference.

Table III. Thermal conductivity data of Ca₂Fe₂O_{6-δ} and Sr₂Fe₂O_{6-δ} at room temperature.

Ca ₂ FeMnO _{6-δ}	Sr ₂ FeMnO _{6-δ}
0.45 ± 0.098 (Wm ⁻¹ K ⁻¹)	0.36 ± 0.095 (Wm ⁻¹ K ⁻¹)

The study underscores the interplay of phonons and radiation in determining thermal conductivity, with oxygen vacancies identified as a key factor. The presence of oxygen vacancies increases phonon scattering, suppressing lattice thermal conductivity. The difference in thermal conductivity between Ca₂FeMnO_{6-δ} and Sr₂FeMnO_{6-δ} suggests a role for vacancy arrangements and grain boundaries in shaping their thermal properties. Random vacancy distribution and increased grain boundaries help reduce thermal conductivity. Overall, the findings provide crucial insights into the design of materials with tailored thermal properties, with implications for applications requiring efficient thermal insulation.

Acknowledgments

This work is supported in part by the National Science Foundation Tribal College and University Program Instructional Capacity Excellence in TCUP Institutions (ICE-TI) award # 2225648. A part of this work is also supported by NSF grant no. HRD 1839895. Additional support for the work came from ND EPSCOR STEM grants for the purchase of a potentiostat and X-ray diffractometer and the American Indian College Fund for the thermal conductivity meter. The views expressed are those of the authors and do not necessarily represent those of United Tribes Technical College.

Funding

Instructional Capacity Excellence in TCUP Institutions (ICE-TI) award # 2225648 and NSF Tribal Enterprise Advancement Center award grant no. HRD 1839895.

ORCID

Ram Krishna Hona  <https://orcid.org/0000-0002-7436-809X>

References

1. Y. Guo, S. Feng, Y. Yang, R. Zheng, Y. Zhang, J. Fu, H. Wang, and J. Li, "High-entropy titanate pyrochlore as newly low-thermal conductivity ceramics." *J. Eur. Ceram. Soc.*, **42**, 6614 (2022).
2. H. Lee, S. Yang, S. Wi, and S. Kim, "Thermal transfer behavior of biochar-natural inorganic clay composite for building envelope insulation." *Constr. Build. Mater.*, **223**, 668 (2019).
3. D. Liu, Z. Zhou, Y. Wang, and B. Xu, "Highly porous (La_{1/5}Nd_{1/5}Sm_{1/5}Gd_{1/5}Yb_{1/5})₂Zr₂O₇ ceramics with ultra-low thermal conductivity." *Ceram. Int.*, **48**, 26400 (2022).
4. T. Wu and P. Gao, "Development of perovskite-type materials for thermoelectric application." *Materials*, **11**, 999 (2018).
5. S. Tang, M. Wu, S. Bai, D. Luo, J. Zhang, and S. Yang, "Honeycomb-like puckered PbTe monolayer: A promising n-type thermoelectric material with ultralow lattice thermal conductivity." *J. Alloys Compd.*, **907**, 164439 (2022).
6. W. Xu, P.-P. Shang, A. Marcelli, G. Cibin, and J.-F. Li, "Multiple emerging nano-phases are at the origin of the low lattice thermal conductivity of SnSe?" *Mater. Today Phys.*, **24**, 100656 (2022).
7. Q. Liu, K.-F. Liu, Q.-Q. Wang, X.-C. Liu, F. Yu, J. Liu, Y.-Y. Su, and S.-Q. Xia, "Rattling-like scattering behavior in ALiSb (A = Ca, Sr, Eu, Yb) Zintl phases with low thermal conductivity." *Acta Mater.*, **230**, 117853 (2022).
8. R. K. Hona, A. Huq, and F. Ramezanipour, "Unraveling the role of structural order in the transformation of electrical conductivity in Ca₂FeCoO_{6-δ}, CaSrFeCoO_{6-δ}, and Sr₂FeCoO_{6-δ}." *Inorg. Chem.*, **56**, 14494 (2017).
9. R. K. Hona, A. Huq, S. Mulmi, and F. Ramezanipour, "Transformation of structure, electrical conductivity, and magnetism in AA'Fe₂O_{6-δ}, A = Sr, Ca and A' = Sr." *Inorg. Chem.*, **56**, 9716 (2017).
10. R. K. Hona and F. Ramezanipour, "Enhanced electrical properties in BaSrFe₂O_{6-δ} (δ = 0.5): a disordered defect-perovskite." *Polyhedron*, **167**, 69 (2019).
11. S. B. Karki, R. K. Hona, and F. Ramezanipour, "Effect of structure on sensor properties of oxygen-deficient perovskites, A2BB'O5 (A = Ca, Sr; B = Fe; B' = Fe, Mn) for oxygen, carbon dioxide and carbon monoxide sensing." *J. Electron. Mater.*, **49**, 1557 (2020).
12. G. J. Snyder and E. S. Toberer, "Complex thermoelectric materials." *Nature Mater.*, **7**, 105 (2008).
13. R. K. Hona, S. B. Karki, G. Dhaliwal, M. Guinn, and F. Ramezanipour, "High thermal insulation properties of A₂FeCoO_{6-δ} (A = Ca, Sr)." *J. Mater. Chem. C*, **10**, 12569 (2022).
14. R. Kun, S. Populoh, L. Karvonen, J. Gumbert, A. Weidenkaff, and M. Busse, "Structural and thermoelectric characterization of Ba substituted LaCoO₃ perovskite-type materials obtained by polymerized gel combustion method." *J. Alloys and Compd.*, **579**, 147 (2013).
15. L. Chen, Y. Zhang, X. Wang, B. Jalan, S. Chen, and Y. Hou, "Roles of point defects in thermal transport in perovskite barium stannate." *J. Phys. Chem. C*, **122**, 11482 (2018).
16. Z. Li, C. Xiao, H. Zhu, and Y. Xie, "Defect chemistry for thermoelectric materials." *J. Am. Chem. Soc.*, **138**, 14810 (2016).
17. L. Hu, T. Zhu, X. Liu, and X. Zhao, "Point defect engineering of high-performance bismuth-telluride-based thermoelectric materials." *Adv. Funct. Mater.*, **24**, 5211 (2014).
18. Y. Xia and M. K. Y. Chan, "Anharmonic stabilization and lattice heat transport in rocksalt β-GeTe." *App. Phys. Lett.*, **113**, 193902 (2018).
19. J. He, S. N. Girard, M. G. Kanatzidis, and V. P. Dravid, "Microstructure-lattice thermal conductivity correlation in nanostructured PbTe_{0.7}Sn_{0.3} thermoelectric materials." *Adv. Funct. Mater.*, **20**, 764 (2010).
20. T. Tadano, Y. Gohda, and S. Tsuneyuki, "Impact of rattlers on thermal conductivity of a thermoelectric clathrate: a first-principles study." *Phys. Rev. Lett.*, **114**, 095501 (2015).
21. T. Yue, Y. Zhao, J. Ni, S. Meng, and Z. Dai, "Strong quartic anharmonicity, ultralow thermal conductivity, high band degeneracy and good thermoelectric performance in Na₂TlSb." *NPJ Comput. Mater.*, **9**, 17 (2023).
22. X. Song, Y. Zhao, J. Ni, S. Meng, and Z. Dai, "Strong anharmonic phonon scattering and superior thermoelectric properties of Li₂NaBi." *Mater. Today Phys.*, **31**, 100990 (2023).
23. R. K. Hona, S. B. Karki, and F. Ramezanipour, "Oxide electrocatalysts based on earth-abundant metals for both hydrogen- and oxygen-evolution reactions." *Sustain. Chem. Engin.*, **8**, 11549 (2020).
24. K. W. Schlichting, N. P. Padture, and P. G. Klemens, "Thermal conductivity of dense and porous yttria-stabilized zirconia." *J. Mater. Sci.*, **36**, 3003 (2001).
25. P. G. Klemens, "Phonon scattering by oxygen vacancies in ceramics." *Phys. B Condens. Matter*, **263-264**, 102 (1999).